# Deep proteomic analysis of human microglia and model systems reveal fundamental biological differences of *in vitro* and *ex vivo* cells

Amy F Lloyd[1*], Anna Martinez-Muriana[2,3], Pengfei Hou[2,3], Emma Davis[4,5], Renzo Mancuso[6,7], Alejandro J Brenes[1,8], Ivana Geric[2,3], An Snellinx[2,3], Katleen Craessaerts[2,3], Tom Theys[9], Mark Fiers[2,3], Bart De Strooper[2,3,4,5,*], Andrew JM Howden[1,*].

1. Cell Signalling and Immunology, University of Dundee, Dundee, UK
2. VIB Centre for Brain & Disease Research, Leuven, Belgium
3. Department of Neurosciences, Leuven Brain Institute, KU Leuven, Leuven, Belgium
4. The Francis Crick Institute, London, UK
5. UK Dementia Research Institute at UCL, University College London, London, UK
6. Department of Biomedical Sciences, University of Antwerp, Antwerp, Belgium
7. MIND lab, VIB Centre for Molecular Neurology, VIB, Antwerp, Belgium
8. Centre for Gene Regulation and Expression, University of Dundee, Dundee, UK
9. Department of Neurosciences, Research Group Experimental Neurosurgery and Neuroanatomy, KU Leuven, Leuven, Belgium

* Correspondence: alloyd001@dundee.ac.uk (AFL), b.strooper@ukdri.ucl.ac.uk (BDS), a.howden@dundee.ac.uk (AJMH)

## Abstract

Using high resolution quantitative mass spectrometry we have generated in-depth proteome maps of human and mouse *ex vivo* and *in vitro* microglia. We reveal a tenfold difference in protein content of *ex vivo* and *in vitro* cells and fundamental differences in protein expression related to protein synthesis, metabolism, microglia markers and environmental sensors. While human and mouse microglia are different in their proteomes, the species differences are smaller than the changes induced by cell culture. Remarkably, xenografting human microglia derived from human stem cells into mouse brain restores the *in vivo*-like microglia proteomic signature including reduction in the total amount of protein, energy demand and protein synthesis, and re-expression of homeostatic microglia markers. We identify more than 9000 microglia proteins and discuss how they relate to microglia function. This data provides a vital proteomic resource for understanding *in vitro* and *ex vivo* microglia phenotypes.

## Introduction

Microglia, the resident immune cells of the central nervous system (CNS) are the first responders to pathogenic invasion and damage. Developmentally, microglia play critical roles in axon guidance (Pont-Lezica 2014, Squarzoni 2014), synaptic pruning (Stevens 2007, Shafer 2012), supporting neuronal survival (Ueno 2013, Fujita 2014) and myelination (Wlodarczyk 2017). Although post-development, microglia are maintained in a homeostatic state of constant surveillance of their environment, they rapidly activate upon stimulation, adopting a plethora of phenotypes that are mainly defined at the gene expression level. Depending on the stimulus, microglia can range from activating to a potent inflammatory state, to that of a tissue-reparative, inflammatory-resolving state (Miron 2013, Lloyd 2019). Sustained activation of the former is a pathological hallmark of neurodegenerative diseases such as Alzheimer's disease (Hickman 2008, Serrano-Pozo 2013) and

multiple sclerosis (Miron 2013, Lloyd 2019), manifesting a chronic inflammatory environment and progressive neuronal and glial cell death.

Manipulation of *in vitro*, *ex vivo* and *in vivo* models has been critical in our understanding of microglia biology and function, however it is uncertain as to how limiting these models are in our understanding of human microglia biology. Transcriptomic studies have uncovered the heterogenic landscape of murine and human microglia throughout the CNS in health and disease (Olah 2018, Mancuso 2019, Masuda 2019, Chen 2020), yet disparity between the transcriptome and proteome (Johnson 2022) means that much is still to be known about microglia. Proteins are the main mechanistic mediators of cell phenotypes; however, the microglia proteome remains poorly defined. Uncovering the human microglia proteome and understanding how well experimental models capture the essence of human microglia is of great importance both experimentally and clinically.

To investigate differences between microglia model systems, we used high resolution quantitative mass spectrometry to map the proteomes of *ex vivo* primary human microglia, *ex vivo* primary mouse microglia, human embryonic stem cell (hESC)-derived microglia and the BV2 mouse microglia cell line. We identified and quantified in total over 9400 different microglia proteins. We reveal striking differences between microglia models and their capacity for protein synthesis, energy production and their ability to sense and respond to their environment. Xenografting of human stem cell derived microglia into mouse brains lead to drastic proteomic reprogramming with close resemblance to *ex vivo* human microglia, such that energy demand and protein synthesis scaled back to *ex vivo* levels, and homeostatic microglia markers were re-expressed. This data provides a valuable resource to the field which can be easily interrogated using our web portal https://data.bdslab.org/Lloyd2022 (*trial version available until publication*). Furthermore, this resource details fundamental new insights into the biology of microglia models and will help better understand the role of these cells in health and disease.

## Results

### Proteomics Reveals Fundamental Differences Between *In vitro* And *Ex vivo* Microglia

Quantitative mass spectrometry was used to uncover high-resolution proteomes of *ex vivo* primary human and mouse microglia acutely isolated from brain, *in vitro* hESC-derived microglia and the BV2 mouse microglia cell line. Human microglia were isolated from the healthy rim of surgically resected temporal lobe tissue of epilepsy patients, as previously described (Mancuso 2019). To generate a deep microglia proteome for each subset, samples were highly fractionated by high-performance liquid chromatography (HPLC) into 16 fractions prior to mass spec analysis, enabling a more in-depth proteome coverage that includes the detection of less abundant proteins, as well as higher accuracy of quantification. A basic overview of the sample handling and processing workflow is presented in Fig. 1a. Raw mass spec files were analysed using MaxQuant (Cox 2008) and searched against either human or mouse databases, with 9840 human and 9602 mouse proteins in total being identified (Supplementary File 1). The average numbers of proteins identified across bio-replicates for each subset varied slightly, with the most proteins detected in BV2 (8284) and *ex vivo* mouse microglia (8132), compared to 7448 for hESC-microglia and 7165 for *ex vivo* human microglia (Fig. 1b). Of these proteins, 5493 were conserved across all microglia samples (Sup Fig. 1a). Gene ontology (GO) analysis indicates glycolysis and antigen presentation among others as important functional categories in the conserved group of proteins (Sup Fig. 1c).

Estimates of absolute protein copy numbers per cell and protein concentrations were calculated by the 'proteomic ruler' method, using the signal intensity of histones as an internal standard (Sup Fig. 1b), as previously described (Wisniewski 2014). Protein mass calculations uncovered striking differences between *in vitro* cultured and *ex vivo* primary microglia, demonstrating a near 10-fold difference in the amount of protein mass between the *in vitro* BV2 and hESC-microglia (~300pg protein per cell) compared to the *ex vivo* mouse and human microglia (~35pg protein per cell) (Fig. 1c). Furthermore, in line with the protein content results, a principal component analysis (PCA) displayed close clustering of replicates from both *ex vivo* groups compared to *in vitro* cultured microglia (Fig. 1d).

To understand the considerable difference in protein content between microglia subsets we next evaluated the contribution of key biological compartments and cellular machinery to the protein mass of the cell. Proteins associated with glycolysis, mitochondria, ribosomes and nuclear envelope were investigated. Calculating the proportion of the proteome dedicated to these groups demonstrates the importance of each of these processes to each microglia subset. BV2 cells had the greatest level of proteins dedicated to glycolytic activity; more than double that of the other microglia subsets at 3.3% of their total proteome compared to 1.4% in hESC-microglia, 1.5% in *ex vivo* mouse microglia and 0.6% in *ex vivo* human microglia (Fig. 1e, f). BV2 and hESC-microglia also had the highest proportion of their proteomes dedicated to mitochondrial and ribosomal proteins, although BV2 cells were again much higher than other microglia subtypes, suggesting the greatest energy demand and rate of protein synthesis (Fig. 1e, f). Indeed, eukaryotic initiation factor 4 (eIF4) complexes vital for the binding of mRNA to 40S ribosomal subunits for translation (Sup Fig. 1d) are all greatly increased in BV2 and hESC-microglia samples compared to the *ex vivo* microglia (Sup Fig. 1e). Conversely, concentration of translation inhibitor PDCD4 is highest in primary human microglia (Sup Fig. 1e), reflecting their tighter regulation of protein synthesis. Furthermore, one molecule of PDCD4 inhibits two molecules of eIF4A1 to inhibit CAP-dependent translation (Suzuki 2008), and adjusted ratios of PDCD4: eIF4A1 show that *ex vivo* mouse and human microglia have the greatest number of PDCD4 molecules to eIF4A1 molecules, whereas BV2s have the least (Sup Fig. 1f), demonstrating the microglia subsets with the greatest and least regulation of translation, respectively. Although nuclear envelope protein content was greatest in BV2 and hESC-microglia (Fig. 1e), the proportion of the proteome dedicated to these proteins was roughly the same for all subsets (1.4%-2.1%). Altogether, our data demonstrates that *in vitro* microglia have the greatest capacity for protein synthesis and energy production, which is likely to sustain their considerable protein mass.

**Quantitative Mass Spectrometry Defines the Human Microglia Proteome**

Given the intense interest in microglia in health and disease, we used our in-depth proteomic data to define the *ex vivo* human microglia proteome. Microglia were isolated from 5 amygdalo-hippocampectomy patients, and we detected on average 7165 proteins across the individuals (Sup Fig. 2a) with an average total protein mass per cell of 37pg (Sup Fig. 2b). Most proteins detected (4830) were expressed in all 5 patient samples (Sup Fig. 2c) showing high proteomic conservation across patients. The top 100 most abundant *ex vivo* human microglia proteins were grouped by their GO term biological processes, allowing us to evaluate the contribution of key processes to the cell (Fig. 2a). The most abundant proteins are predominantly histone and actin-associated proteins (Fig. 2a). Interestingly, proteins associated with immune responses, sensome and glycolysis are also some of the most abundant proteins, along with phagosome and iron-storage proteins (Fig. 2a) showing the wide diversity of cellular and molecular functions in human microglia. In particular, the

calprotectin subunits S100A8 and S100A9 and ferritin heavy chain (FTH1) are among the top 20 most abundant proteins (Sup Fig. 2d), further highlighting the importance of these proteins and their roles in both inflammatory regulation and iron storage and metabolism in human microglia. Proteins detected in a minimum of 3 out of 5 samples were then analysed further with the top 10 most enriched GO terms associated with 'molecular function', 'cellular component' and 'biological process' identified (Fig. 2b). Significantly enriched GO terms include those associated with antigen presentation, transcriptional regulation and proteasome activity (Fig. 2b). Taken together this data shows the most important aspects of human microglia biology and function.

Comparisons of *ex vivo* mouse and human microglia showed that thousands of proteins were differentially expressed, with 1014 and 711 proteins being significantly enriched in the human and mouse microglia, respectively (Fig. 2c, T-Test p-value <0.05 ($-\log_{10}$ P-value >1.3) and fold change >2 ($\text{Log}_2$ fold change >1 or <-1)). Significantly enriched proteins in human microglia included antigen presentation protein CD74 and APOE receptor SORL1 (Fig. 2c). GO term analysis showed significant engagement of FC receptor activation, phagocytosis and inflammatory responses in enriched human microglia proteins (Sup Fig. 2e), suggesting that human microglia may be more primed for activation and inflammation than mouse microglia. Furthermore, 262 and 268 unique proteins were identified in *ex vivo* mouse and human samples, respectively (Fig. 2d). Of these unique proteins, immune and inflammatory associated proteins including IGF-1, C3 and CD40 were detected in human samples, whereas proteins associated with cellular fate (NOTCH1/2) and microglia homeostasis (SMAD1) were present in mouse microglia. Proteins involved in amyloid-β processing including APOE, CLU and SORL1, all major risk genes for Alzheimer's, are significantly higher in human microglia samples compared to mouse (Fig. 2e), as well as inflammatory proteins IL-18 and CD45 (PTPRC) (Fig. 2f). This data suggests that human microglia have greater basal activation than mouse microglia. This may highlight how fundamental differences in the human and mouse genome shape microglia phenotypes.

### *In vitro* Microglia Lack Key Markers that Define Microglia Identity

Increased machinery for glycolysis and protein production in the *in vitro* microglia samples suggests striking differences between *in vitro* and *ex vivo* microglia biology. The observed 10-fold difference in protein content between *in vitro* and *ex vivo* cells was also reflected in the copy numbers of most proteins. This was evident when comparing fold change differences in absolute protein copy numbers between an *in vitro* and an *ex vivo* subset, for example, BV2s compared to *ex vivo* mouse microglia (Sup Fig. 3a), as the majority of proteins detected were found at higher abundance in the BV2s. Given the considerable difference in total protein mass between *in vitro* and *ex vivo* populations, we calculated the concentration of each protein using the histone ruler to normalise for total protein mass (Sup Fig. 3b). Lower protein content of *ex vivo* cells was not due to the method used for their isolation and processing, as BV2 cells that underwent fluorescence-activated cell sorting (FACS), like the *in vivo* cells, showed no differences in protein content (Sup Fig. 3c), nor proteins identified after sorting (Sup Fig. 3d, e) compared to unsorted cells. There are instances in which copy numbers are a more appropriate comparison, such as when looking at protein interactions with inhibitors (Sup Fig. 1f), and therefore both protein copy number and concentration are used.

Increases in energy demand and protein synthesis may suggest an activated microglia phenotype (Lauro 2020), also defined by decreases in homeostatic protein expression and increases in phagocytosis receptor expression (Fig. 3a). To explore this further, expression of key microglia

markers were investigated in each subset, and markers associated with homeostasis (P2RY12, TMEM119) were abundantly higher in *ex vivo* human and mouse microglia compared to *in vitro* microglia (Fig. 3b). Moreover, IRF8 and PU.1 (SPI1), transcription factors central to microglia cell identity and function were also higher in *ex vivo* cells, along with most other microglia-associated markers (Fig. 3b). P2RY12, TMEM119 and CX3CR1 were not detected in any biological replicates for BV2 microglia and expressed at very low abundance in hESC-microglia (Fig. 3b). Although a lack of microglia marker protein expression could suggest a lack of microglia identity, it may also represent an activated microglia phenotype, as both P2RY12 and TMEM119 are downregulated in microglia in response to inflammatory stimuli (Zrzavy 2017) and neurodegeneration (Keren-Shaul 2017, Krasemann 2017, Kenkhuis 2022). Indeed, microglia/macrophage phagocytosis marker CD68 is expressed in all four microglia subsets, supporting a microglia identity in each, however expression is drastically higher in BV2 microglia suggestive of activation (Fig. 3c). Expression of the transporter SLC2A5 is associated with homeostatic microglia and was only detected in *ex vivo* primary mouse and human microglia (Fig. 3d). Conversely, SLC2A6, a lysosomal transporter shown to modulate glycolysis in inflammatory macrophages (Maedera 2018) and increase expression upon LPS stimulation (Caruana 2019), is only detected in BV2 and hESC-microglia (Fig. 3e), further supporting an activated *in vitro* phenotype, and consistent with the increased glycolytic activity of *in vitro* microglia (Fig. 1e, f).

Activation of the transforming growth factor beta (TGF-β) pathway has been associated with maintenance of microglia homeostasis in mice (Suzumura 1993, Butovsky 2013, Zoller 2018) via engagement and phosphorylation of SMAD proteins that translocate to the nucleus and bind to TGF-β response elements (Fig. 3f), inducing expression of inflammatory modulators (Zoller 2018). Expression of TGF-β receptors TGFBR1 and TGFBR2 was highest in *ex vivo* mouse microglia (Fig. 3g, h), as well as expression of SMAD3 (Fig. 3j), however SMAD2 and 4 were similar across microglia subtypes (Fig. 3i, k). Interestingly, engagement of the TGF-β pathway was low in primary human microglia, suggesting that although TGF-β pathway induction is important for mouse microglia homeostasis, its importance for human microglia homeostasis is unclear. Low TGF-β pathway engagement may also suggest that primary human microglia are more activated, as indicated by lower expression of P2RY12 and TMEM119 (Fig. 3b) and increases in inflammatory proteins (Fig. 2f).

### *In vitro* Cultured hESC-microglia Show a Pronounced DAM Signature

Activation of microglia is a prominent feature of neurodegenerative diseases such as Alzheimer's disease (AD). In response to AD-associated changes and cellular damage, a subset of microglia undergo a two-step transformation from their homeostatic state by expression of particular gene signatures, firstly in a TREM-2 independent (Stage 1) and then TREM-2 dependent (Stage 2) manner (Keren-Shaul 2017) (Fig. 4a). Loss of homeostatic markers P2RY12, TMEM119 and CX3CR1 are indicative of microglia activation, and indeed all three of these proteins are present in *ex vivo* mouse and human microglia, but not found in BV2 microglia and barely detectable in hESC-microglia (Fig. 4b). Interestingly, expression of the majority of Stage 1 and Stage 2 DAM signature proteins are highest in hESC-microglia, including APOE, B2M, CTSB, CTSD, TYROBP, CD9, CSF1, ITGAX, LIPA, LPL, TIMP2 and TREM2 (Fig. 4c, d). Although BV2 microglia have undetectable levels of homeostatic microglia proteins (Fig. 4b), expression of the majority of DAM-related proteins in BV2s was overall as low as *ex vivo* microglia with the exception of CLEC7A, ITGAX and LILRB4 (Fig. 4c, d). This data highlights a basal level of activation in these *in vitro* cultured microglia, in particular the similarities of hESC-derived microglia to that of the activated and inflammatory DAM microglia phenotype.

**The Microglia Sensome: *Ex vivo* Primary Microglia are Primed to Sense and Respond to Environmental Changes**

One of the most important microglia functions is the sensing and surveillance of their surrounding environment to maintain CNS homeostasis (Li 2018). Microglia therefore express a wide array of receptors suited to the detection of a range of stimuli. For example, detection of ATP and nucleotides released from dying cells can stimulate microglia migration towards the area of damage and promote clearance of debris (Davalos 2005, Haynes 2006) (Fig. 5a). Indeed, the lack of P2RY12 and CX3CR1 expression in the *in vitro* microglia is in dramatic contrast to *ex vivo* primary mouse and human microglia (Fig. 3b, 4b) which as well as being an indicator of activation, also demonstrates that *in vitro* microglia lack some of the proteins required to sense and respond to their environment. Microglia also play a key role in the sensing and removal of extracellular glutamate from synaptic junctions via SLC1A2 (Xing 2009). The glutamate transporter is expressed highest in *ex vivo* mouse and human microglia, while undetected in BV2 cells (Fig. 5b). Complement receptor activation relies on complement ligand engagement, such as C3, found on surface of pathogens or synapses destined to be cleared (Stevens 2007, Hong 2016). Although C3 was found at the highest concentration in *ex vivo* human microglia (Fig. 5c), its receptor C3AR1 was most highly expressed in hESC-microglia (Fig. 5d), suggesting differences in the release and detection of complement proteins in these subtypes. Toll-like receptors (TLRs) are vital for the detection of foreign bodies such as components of bacterial cell walls (via TLR4) and double-stranded viral RNA (via TLR3) (Fig. 5e). Copies of TLR3 were lowest in BV2s yet were present in the thousands of copies in all other microglia subsets. Interestingly, TLR4 was absent in *ex vivo* human microglia and barely detectable in *ex vivo* mouse microglia, although upregulation of this receptor has been associated with pro-inflammatory microglial activation (Cui 2020) and is indeed expressed highly by *in vitro* microglia (Figure 5e), further supporting an activated phenotype in these cells.

As well as sensing the environment, microglia also need to sense and take up extracellular nutrients vital to their function. Such nutrient receptors include those responsible for the uptake of glucose, lactate, amino acids and various solutes important for mitochondrial function and metabolism. Copies of the lactate transporter SLC16A1 were strikingly high in BV2 microglia, with lowest expression in *ex vivo* microglia (Fig. 5f). This may be due to the increased glycolytic activity of BV2s and the release of lactate as a waste product that needs to be cleared. However, there is emerging evidence that microglia may also use lactate as an alternative fuel (Monsorno 2022). Differential expression of glucose transporters SLC2A5 and SLC2A6 in the *ex vivo* and *in vitro* microglia, respectively, are also presented in their copy numbers here (Fig. 5f). Disparity between *in vitro* and *ex vivo* microglia was also observed by their expression of amino acid transporter SLC7A5. Interestingly, SLC7A5 has been implicated in metabolic reprogramming of pro-inflammatory microglia via leucine influx and its influence on microglia glycolytic activity (Yoon 2018). SLC7A7, a leucine/ arginine amino acid transporter associated with microglia precursor identity (Rossi 2015), was found in all microglia subsets except for *ex vivo* human microglia. Mitochondrial solute transporters SLC25A3 and SLC25A5, associated with NLRP3 and inflammasome activation in microglia (Pollock 2020) were both most highly expressed in BV2 microglia (Fig. 5f). However, SLC25A5 was still expressed at hundreds of thousands of copies in *ex vivo* and hESC-microglia and is likely an important mitochondrial transporter in all microglia subsets. This data highlights the diversity of metabolic programming present in these microglia subsets, reflective of their environment, nutrient availability and potentially their activation state. Overall, evidence suggests that *ex vivo* microglia may be able to respond to a wider range of stimuli from their surrounding microenvironment, most likely shaped by the heterogeneity of the stimuli they face, compared to *in vitro* microglia.

### Xenografted hESC-microglia into Mouse Brain Induces an '*In vivo*-Like' Microglia Signature Compared to *In vitro* Cultured hESC-microglia

Although *in vitro* cultures are more amenable to pharmacological and experimental manipulation, it is perhaps unsurprising that the *in vitro* environment creates fundamental biological differences in cells compared to their *in vivo*/ *ex vivo* counterparts. Efforts to overcome this by generating xenografts from *in vitro* human derived cells in model organisms create a promising avenue to understand human cellular responses to disease models. Indeed, engraftment of human stem cell derived microglia into mouse brains has been successfully developed (McQuade 2018, Mancuso 2019), with xenografted hESC-derived microglia adopting a homeostatic phenotype compared to *in vitro* cultured hESC-derived microglia (Mancuso 2019). To understand these changes at the protein level and to further explore the impact of *in vivo* environment on *in vitro* cells, we compared the proteomes of *in vitro* cultured hESC-derived microglia, mouse brain xenografted hESC-derived microglia and *ex vivo* human primary microglia (Fig. 6a). PCA analysis of all microglia subsets revealed that xenografted hESC-microglia clustered much closer to *ex vivo* microglia than to their *in vitro* counterparts (Fig. 6b), suggesting greater proteomic similarities to *ex vivo* microglia. Most striking is that the xenografted hESC-microglia, similarly to *ex vivo* human microglia, have approximately 10-fold lower protein content compared to *in vitro* hESC-microglia (Fig. 6c). The proportion of the xenografted hESC-microglia proteome dedicated to glycolysis (Fig. 6d), mitochondria proteins (Fig. 6e) and ribosomal proteins (Fig. 6f) was also reduced to proportions similar to *ex vivo* primary human microglia. Furthermore, comparisons of differentially expressed proteins between *in vitro* hESC-microglia, xenografted hESC-microglia and *ex vivo* primary microglia (Fig. 6g, Sup Fig. 4a) demonstrate a significantly enriched homeostatic protein signature in the xenografted cells compared to both *in vitro* hESC-microglia and *ex vivo* human microglia (Fig. 6g). Interestingly, xenografted cells also displayed a significant downregulation of DAM-associated proteins compared to both *in vitro* hESC-microglia and *ex vivo* human microglia (Fig. 6g). However, there were notably fewer differentially expressed proteins between xenografted hESC-microglia and *ex vivo* human microglia, suggesting a closer similarity between these cells (Fig. 6g). Furthermore, upon engraftment in the mouse brain, hESC-microglia re-express homeostatic microglia markers TMEM119, P2RY12 and CX3CR1 to similar or higher concentrations than *ex vivo* human microglia (Fig. 6h-j). This is concurrent with RNA sequencing data comparing the same microglia subsets that also showed restoration of a homeostatic marker expression after xenograftment (Mancuso 2019). Altogether this data showcases the importance of environment on microglia biology and marker expression, as well as further supporting the use of xenograft models to study human microglia dynamics in health and disease.

## Discussion

While microglia are critical for the maintenance of brain homeostasis, they also play a central role in neuroinflammatory and neurodegenerative diseases. To fully understand their role in pathological conditions we must understand how their identity and function shifts from homeostatic to pathological states. Here we define the human microglia proteome and provide essential proteomic resources characterising the most commonly used model systems to study microglia dynamics. We have identified a total of 9456 human proteins and 9629 mouse proteins, highlighting comprehensive proteomic coverage of all microglia datasets. Data is available via our online searchable database https://data.bdslab.org/Lloyd2022 (*trial version available until publication*).

One highlight is the fundamental proteomic differences between *in vitro* and *ex vivo* microglia, a dichotomy much more apparent than mouse vs human. Striking differences in protein content of cells, metabolic demand and protein synthesis between *in vitro* and *ex vivo* microglia demonstrate the extent of environmental influence on cell biology and behaviour. Indeed, components of culture media increase mitochondrial mass of cells (Minarrieta 2021), with foetal bovine serum (FBS) directly linked to inducing metabolic reprogramming in cells via the Warburg effect (Steenbergen 2018, Chelladurai 2021). BV2 cells have at least ~3-fold higher glycolytic protein content than all other microglia subtypes, being the only cells cultured in media supplemented with FBS. Although hESC-derived microglia are not cultured in FBS, a wide range of cytokines and growth factors support their survival and differentiation into microglia, and therefore the influence of these factors on their metabolic programming should be considered. Both *in vitro* microglia subsets demonstrate a 10-fold greater protein content compared to the *ex vivo* subsets, along with significantly higher glycolytic, mitochondrial and ribosomal protein content; likely a consequence of the nutrient-rich culture environment devoid of competition from other cell types. Indeed, we addressed that these differences were not due to differences in cell preparation or isolation, as *in vitro* BV2 cells were subjected to both direct lysis and FACS, with no changes in protein content, nor protein identification observed.

To define the human microglia proteome we investigated their most abundant proteins which are involved in wide ranging functions associated with immune responses, glycolysis, RNA splicing (spliceosome), iron storage and lipid metabolism to name a few. Evidence that homeostatic microglia use both glycolysis and oxidative phosphorylation has been shown previously (Zhang 2014) and is supported at the protein level here. The diversity of proteins expressed reflects the diverse environmental stimuli that microglia function in and respond to. This may be particularly relevant when comparing *ex vivo* human and mouse microglia. Significantly enriched proteins in human microglia show not only an enrichment in immune response proteins, but also proteins associated with amyloid-β processing and neurofibrillary tangles. An increased basally activated phenotype in human microglia may explain the lack of TGFβ signalling pathway engagement compared to mouse microglia, yet both *ex vivo* microglia subsets express proteins associated with homeostasis (P2RY12, TMEM119). This is in stark contrast to the *in vitro* microglia subsets which not only lack expression of homeostatic microglia proteins, but also express the glucose transporter SLC2A6 associated with upregulation upon LPS stimulation (Caruana 2019). The lack of microglia marker expression in *in vitro* microglia subsets puts into question the true identity and function of these microglia cells, and if, at all, they can model the complex biology and behaviour of *in vivo* microglia.

A particularly interesting finding centred around the disease associated microglia (DAM) signature found in the *in vitro* hESC-derived microglia. DAM microglia are also characterised by reduction of homeostatic marker expression (Keren-Shaul 2017), consistent with the hESC-microglia proteome. This activated phenotype of the hESC-microglia, although not fully understood, may also explain the lack of sensome associated protein expression, as *in vitro* activated microglia have been shown to reduce their cellular motility and sensing of their surrounding environment (Koss 2019). These *in vitro* microglia subsets lack the machinery to sense and interact with a heterogenous *in vivo* environment, having never been exposed to such diversity of cell types and stimuli. This put into question whether such a phenotype could be reprogrammed in *in vitro* cells if their environment changed. For this we utilised the hESC-microglia/ mouse brain xenograft model recently developed (Mancuso 2019) to compare how the hESC-microglia proteome changes from *in vitro* culture to the *in vivo* environment. It was immediately evident that the *in vivo* environment drastically changes the biology of hESC-microglia; their total protein content reduced 10-fold to levels similar to *ex vivo* human microglia, and PCA analysis grouped xenografted hESC samples much closer to the *ex vivo*

human microglia than their *in vitro* counterparts. Like *ex vivo* human microglia, xenografted hESC-microglia expressed high levels of homeostatic microglia proteins and had similar proportions of their proteomes dedicated to energy demand and protein synthesis. This is in line with previous single cell RNA sequencing of *in vitro* and xenografted hESC-microglia also demonstrate a restoration in microglia homeostatic signatures in xenografted microglia (Mancuso 2019). This signature is also seen at the protein level, further implicating the importance of this model in studying human neurodegenerative diseases.

This data demonstrates the importance of the microglia environment and the limitations of *in vitro* microglia cultures. Furthermore, our data provide the first large scale proteomic characterisation of human microglia and microglia model systems, demonstrating the importance and consequences of the microglia environment on behaviour and function.

## Methods

### Human Samples and Isolation of Primary Human Microglia by FACS

Human primary microglia were isolated from brain tissue samples resected from the temporal cortex during neurosurgery. All samples represented lateral temporal neocortex and were obtained from patients who underwent amygdalo-hippocampectomy for mesial temporal lobe seizures. The mesial temporal specimens were sent to pathology and thus not available for study purposes. Samples were collected at the time of surgery and immediately transferred to the lab for tissue processing, with post sampling intervals of 5-10 min. All procedures were conducted to protocols approved by the local Ethical Committee (protocol number S61186). Brain biopsies were placed in PBS 2%, FCS, 2mM EDTA (FACS buffer), mechanically triturated and enzymatically dissociated using the Neural Tissue Dissociation Kit (P) (Miltenyi) following manufacturer specifications. Then, samples were passed through a cell strainer of 70µm mesh (70µm strainers, Grenier BioOne) with FACS buffer, and centrifuged twice at 300g for 15 min at 4°C. Next, cells were resuspended in 30% Percoll (100% Percoll Plus, 17-5445-02, GE Healthcare) and centrifuged at 300g for 15 min at 4°C. The supernatant and myelin layers were discarded, and the cell pellet was treated to remove red cells (Red blood cell lysis buffer, 420301, Biolegend). After a wash, antibody labelling was performed for 30 min at 4°C, using the anti-CD11b (1:50, 130-113-806, Miltenyi Biotec) and anti-CD45 (1:50, 555485, BD Bioscience), adding e780 (1:2000, 65-0865-14, ThermoFisher) as a cell viability marker. Samples were run on a MACSQuant Tyto cell sorter and data were analysed using FCS express software. Human cells were sorted according to the expression of CD11b, CD45. After isolation, cells were washed two consecutive times with ice cold HBSS, snap frozen, and stored at -80°C.

### Mice

C57BL/6J mice were used to generate *ex vivo* mouse microglia proteomes. For xenotransplant experiments, we used Apphu Rag2−/− IL2rγ−/−hCSF1KI. In brief, Rag2−/− IL2rγ−/−hCSF1KI mice, originally purchased from Jacksons Labs (strain 017708), were crossed with Appem1Bdes mice (MGI ID: 6512851) (abbreviated here Apphu) (Serneels 2020). All animals were bred and housed in groups of 2-3, under a 12 h light/dark cycle at 21°C, with food and water ad libitum in local facilities at KU Leuven. All experiments were conducted according to protocols approved by the local Ethical Committee of Laboratory Animals of the KU Leuven (government license LA1210579, ECD project numbers: P177/2020 and P177/2017) following local and EU guidelines.

**Isolation of Mouse Microglia by FACS**

Male mice were sacrificed at 3.5 months for mouse primary microglia isolation. Mouse primary microglia isolation was performed as previously described (Mancuso 2019). Briefly, mice were terminally anesthetized with an overdose of sodium pentobarbital and transcardially perfused with heparinized PBS. Brains were collected in ice-cold FACS buffer (PBS with 2% FCS and 2mM EDTA). Tissue was mechanically and enzymatically dissociated using the Neural Tissue Dissociation Kit (P) (130-092-628, Mylteni) following manufacturer's instructions. Next, cell suspension was filtered on a 70-µm cell strainer (542070, Greiner) with FACS buffer and centrifuged at 300g for 15 min at 4°C. Cell pellet was further resuspended in 30% Percoll (GE Healthcare) and spun at 300g for 15 min at 4°C. Myelin cleaning was performed by removing myelin layers formed on top of the supernatant with Pasteur pipettes. Then, cell pellet was incubated with fluorophore-conjugated antibodies for 30 minutes at 4°C using anti-mouse CD11b-PE (1: 50, REA592, Miltenyi), anti-mouse CD45-BV421 (1:500, 563890, BD Biosciences) and the cell viability marker e780 (1:2000, 65-2860-40 eBioscience). Microglia were sorted on a Miltenyi MACSQuant Tyto flow cytometer. ~1.5 million sorted microglia (CD11b+/CD45m/e780-) from every two mice were pooled, washed with HBSS and snap frozen for the downstream experiments.

**Culture of BV2 cells**

BV2 cells were cultured in RPMI 1640 (Gibco) with 10% foetal bovine serum (FBS) at 37°C with 5% $CO_2$, with passaging every 2-3 days with trypsin/EDTA (Gibco). 3 biological replicates were generated for proteomic analysis, each with $1x10^6$ cells per sample. Samples were collected by direct lysis on plate in 5% SDS, pipetted into 1.5ml eppendorfs, snap frozen and stored at -80°C.

**Generation of Human-derived Microglia from ESCs**

Human microglia/macrophage precursors were generated from human embryonic stem cells (H9) using the MIGRATE protocol (Fattorelli 2021). On days 25 and 32, precursor cells and embryoid bodies (EBs) were harvested and passed through a sterile reversible cell strainer (37 µm). Only precursor cells will pass through the strainer and EBs will be retained and re-plated for later collections as detailed (Fattorelli 2021). Precursor cells were centrifuged for 5 min at 300 g. Pelleted cells were further resuspended and plated in glass coverslips in a seeding concentration of 10^6 cells/well in microglia differentiation media (TIC) as previously described (Mancuso 2019) and based on previous protocols (Abud et al., 2017; Bohlen et al., 2017). TIC media was composed of phenol-red free DMEM/F12, N-acetylcysteine (5 µg/ml), insulin (1:2,000), Apo-Transferrin (100 µg/ml), sodium selenite (100 ng/ml), cholesterol (1.5 µg/ml) and heparan sulfate (1 µg/ml) supplemented with interleukin-34 (50 ng/ml), macrophage colony stimulating factor (M-CSF) (50 ng/ml), CX3CL1 (10 ng/ml) and transforming growth factor-β (TGF-β)( 25 ng/ml). Microglia were differentiated in TIC media for 7 days and fully refreshed 3 days after plating. To harvest human-derived microglia for proteomics, on day 7 of differentiation, TIC media was removed and cells were washed twice with DPBS. Next, cells were directly lysed on the plate with 5% SDS in DPBS, scrapped off, transferred to a 1.5ml Eppendorf, snap frozen and stored at -80°C.

**Transplantation of Human Microglia into the Mouse Brain**

Generation and grafting of human-derived microglia was performed as previously described (Mancuso 2019, Fattorelli 2021). In brief, day 18 microglia/macrophage progenitors were collected and grafted into ApphuRag2−/− IL2rγ−/−hCSF1KI mice brains at a concentration of 250,000 cells/µl at postnatal day 4 (P4). After injections, mice were left recovering in a heating pad and transferred back to their cages. After 10 weeks, mice were sacrificed, perfused and brain tissue processed for FACS as described above and previously (Mancuso 2019). Samples were stained with the following antibodies: CD11b-PE (1:50, REA592, Miltenyi), anti-human CD45 (1:50, 555485, BD Biosciences), anti-mouse CD45-BV421 (1:500, 563890, BD Biosciences) and cell viability marker e780 (1:2000, 65-2860-40 eBioscience). Microglia were sorted on a Miltenyi MACSQuant Tyto flow cytometer. Between 8.5x10^5 and 1.3x10^6 microglia were sorted per sample (CD11b+/hCD45+/mCD45-/e780-), washed with HBSS and snap frozen for downstream proteomic processing.

**Proteomics Sample Preparation**

All samples were lysed in 400µl lysis buffer (5% SDS, 10mM TCEP, 50mM TEAB) and shaken at RT for 5 minutes at 1000rpm, followed by boiling at 95°C for 5 minutes at 500rpm. Samples were then shaken again at RT for 5 minutes at 1000rpm before being sonicated for 15 cycles of 30 seconds on/ 30 seconds off with a BioRuptor (Diagenode). Benzonase was added to each sample and incubated at 37°C for 15 minutes to digest DNA. Samples were then alkylated with 20mM iodoacetamide for 1 hour at 22°C. Protein concentration was determined using EZQ protein quantitation kit (Invitrogen) as per manufacturer instructions. Protein isolation and clean up was performed using S-TRAP™ (Protifi) columns before digestion with trypsin at 1:20 ratio (enzyme:protein) for 2 hours at 47°C. Digested peptides were eluted from S-TRAP™ columns using 50mM ammonium bicarbonate, followed by 0.2% aqueous formic acid and 50% aqueous acetonitrile containing 0.2% formic acid. Eluted peptides were dried down overnight.

**Peptide Fractionation**

Dried peptides were rehydrated in 210µl 5% formic acid, shaking at 1000rpm for 1 hour at 30°C. Samples were loaded into the high-performance liquid chromatographer (HPLC) with the following buffers: buffer A (10mM ammonium formate with 2% acetonitrile in Milli-Q water (v/v)) and buffer B (10mM ammonium formate with 80% acetonitrile in Milli-Q water (v/v)). Samples were fractionated using high pH reverse phase liquid chromatography using a Dionex Ultimate3000 system. Peptides were loaded onto a 2.1 mm x 150 mm XBridge Peptide BEH C18 column with 3.5 µm particles (Waters) and were separated using a 25 min multistep gradient of solvents A (10 mM formate at pH 9 in 2% acetonitrile) and B (10 mM ammonium formate pH 9 in 80% acetonitrile), at a flow rate of 0.3 mL/min. Samples were fractionated into 16 samples and collected into 96 well plates, with blank samples run between samples. All samples were then dried down overnight before resuspension in 5% formic acid.

**Mass Spectrometry**

For each sample, 2 µg peptide was analysed. Peptides were injected onto a nanoscale C18 reverse-phase chromatography system (UltiMate 3000 RSLC nano, Thermo Scientific) and electrosprayed

into an Q Exactive™ Plus Hybrid Quadrupole-Orbitrap™ Mass Spectrometer (Thermo Fisher). For liquid chromatography the following buffers were used: buffer A (0.1% formic acid in Milli-Q water (v/v)) and buffer B (80% acetonitrile and 0.1% formic acid in Milli-Q water (v/v). Samples were loaded at 10 µL/min onto a trap column (100 µm × 2 cm, PepMap nanoViper C18 column, 5 µm, 100 Å, Thermo Scientific) equilibrated in 0.1% trifluoroacetic acid (TFA). The trap column was washed for 3 min at the same flow rate with 0.1% TFA then switched in-line with a Thermo Scientific, resolving C18 column (75 µm × 50 cm, PepMap RSLC C18 column, 2 µm, 100 Å). Peptides were eluted from the column at a constant flow rate of 300 nl/min with a linear gradient from 3% buffer B to 6% buffer B in 5 min, then from 6% buffer B to 35% buffer B in 115 min, and finally to 80% buffer B within 7 min. The column was then washed with 80% buffer B for 4 min and re-equilibrated in 3% buffer B for 15 min. Two blanks were run between each sample to reduce carry-over. The column was kept at a constant temperature of 50°C.

The data was acquired using an easy spray source operated in positive mode with spray voltage at 2.445 kV, and the ion transfer tube temperature at 250°C. The MS was operated in DDA mode. A scan cycle comprised a full MS scan (m/z range from 350-1650), with RF lens at 40%, AGC target set to custom, normalised AGC target at 300, maximum injection time mode set to custom, maximum injection time at 20 ms and source fragmentation disabled. MS survey scan was followed by MS/MS DIA scan events using the following parameters: multiplex ions set to false, collision energy mode set to stepped, collision energy type set to normalized, HCD collision energies set to 25.5, 27 and 30, orbitrap resolution 30000, first mass 200, RF lens 40, AGC target set to custom, normalized AGC target 3000, maximum injection time 55 ms.

**Proteomics Data Handling, Processing and Analysis**

The data were processed, searched and quantified with the MaxQuant software package (Version 1.6.10.43). Raw mass spec data files for human microglia were searched against a human SwissProt database with isoforms (July 2020) while mouse microglia samples were searched against a SwissProt database with isoforms combined with mouse TrEMBL entries with protein level evidence available and a manually annotated homologue within the human SwissProt database (June 2020). The false discovery rate was set to 1% for positive identification at the protein and peptide-to-spectrum match level. Protein N-terminal acetylation and methionine oxidation were set as variable modifications and carbamidomethylation of cysteine residues was selected as a fixed modification. Match between runs was disabled. The dataset was filtered to remove proteins categorized as ‘contaminants’, ‘reverse’ and ‘only identified by site’. Copy numbers were calculated as described previously (Wisniewski et al., 2014) using Perseus software (MaxQuant).

**Statistical Analysis**

P values were calculated via a two-tailed, unequal variance t-test on log-normalized data. Proteins with P values less than 0.05 were considered significant. Fold-change thresholds were established using a change cut-off greater than 2 or less than 0.5 (ie, a 2-fold change minimum). The mass of individual proteins was estimated using the following formula: $CN \times MW / N_A$ =protein mass (g $cell^{-1}$), where CN is the protein copy number, MW is the protein molecular weight (in Da) and $N_A$ is Avogadro’s Constant. Heat maps were generated using the Morpheus tool from the Broad Institute (https://software.broadinstitute.org/morpheus). PCA plots and Venn diagrams were generated in R

studio. Volcano plots in Supplementary Figure 3a and b were generated using Graphpad Prism. All other volcano plots were generated in R studio using the Limma-Voom package.

### Data Availability

Raw mass spectrometry files and results files will be made available through ProteomeXchange upon publication of this manuscript.

## Acknowledgements

This work was supported by the UK-DRI grant contributed by MRC (UK). Further funding from Fonds voor Wetenschappelijk Onderzoek (FWO, Belgium), ‘‘Methusalem’’ and ‘‘Opening the Future’’ grants from KU Leuven (Belgium), Stichting Alzheimer Onderzoek (Belgium), the Alzheimer Association (USA), the European Research Council ERC-CELLPHASE_AD834682 (EU), Geneeskundige Stichting Koningin Elisabeth (Belgium), Bax-Vanluffelen (Belgium) and Mission Lucidity (Leuven, Belgium). Schematics in all figures were generated with BioRender.com.

## Author Contributions

A.F.L conceived and designed the study, carried out the experiments, analysed and interpreted the data and wrote the manuscript. A.M.M generated *in vitro* hESC-derived microglia for proteomics, carried out xenograft experiments and generated xenograft microglia for proteomics. P.H isolated *ex vivo* mouse microglia for proteomics. E.D assisted in data analysis, generation of figures and development of online database. R.M, A.S and K.C isolated *ex vivo* human microglia for proteomics. A.J.B assisted in data analysis and manuscript preparation. I.G assisted with generating xenograft and *in vitro* hESC-derived microglia samples for proteomics. T.T carried out amygdalo-hippocampectomy surgeries which generated *ex vivo* human microglia samples. M.F assisted in data analysis, data interpretation and development of online database. B.D.S co-supervised the project, co-designed the study and guided experiment design, data interpretation and manuscript preparation. A.J.M.H co-supervised the project, co-designed the study and guided experiment design, data interpretation and manuscript preparation.

## References

Butovsky, O. J., MP. Moore, CS. Cialic, R. Lanser, AJ. Gabriely, G. Koeglsperger, T. Dake, B. Wu, PM. Doykan, CE. Fanek, Z. Liu, L. Chen, Z. Rothstein, JD. Ransohoff, RM. Gygi, SP. Antel, JP. Weiner, HL. (2013). "Identification of a unique TGF-β–dependent molecular and functional signature in microglia." Nature Neuroscience **17**: 131-143.

Caruana, B. B., FL. Knights, AI. Guinlan, KGR. Hoehn, KL. (2019). "Characterisation of Glucose Transporter 6 in Lipopolysaccharaide-Induced Bone Marrow-Derived Macrophage function." The Journal of Immunology **202**: 1826-1832.

Chelladurai, K. C., JDS. Rajagopalan, K. Yesudhason, BV. Venkatachalam, S. Mohan, M. Vasantha, NC. Christyraj, JRSSC. (2021). "Alternative to FBS in animal cell culture - An overview and future perspective." Heliyon **7**(8).

Chen, W. L., A. Craessaerts, K. Pavie, B. Sala Frigerio, C. Corthout, N. Qian, X. Lalakova, J. Kuhnemund, M. Voytyuk, I. Wolfs, L. Mancuso, R. Salta, E. Balusu, S. Snellinx, A. Munck, S. Jurek, A. Fernandez Navarro, J. Saido, TC. Huitinga, I. Lundeberg, J. Fiers, M. De Strooper, B. (2020). "Spatial Transcriptomics and In Situ Sequencing to Study Alzheimer's Disease." Cell **182**(4): 976-991.

Cox, J. M., M. (2008). "MaxQuant enables high peptide identification rates, individualized p.p.b.-range mass accuracies and proteome-wide protein quantification." Nature Biotechnology **26**: 1367-1372.

Cui, W. S., C. Ma, Y. Wang, S. Wang, X. Zhang, Y. (2020). "Inhibition of TLR4 Induces M2 Microglial Polarization and Provides Neuroprotection via the NLRP3 Inflammasome in Alzheimer's Disease." Front Neurosci.

Davalos, D. G., J. Yang, G. Kim, JV. Zuo, Y. Jung, S. Littman, DR. Dustin, ML. Gan, W. (2005). "ATP mediates rapid microglial response to local brain injury in vivo." Nature Neuroscience **8**(6): 725-758.

Fattorelli, N. M.-M., A. Wolfs, L. Geric, I. De Strooper, B. Mancuso, R. (2021). "Stem-cell-derived human microglia transplanted into mouse brain to study human disease." Nature Protocols **16**(2): 1013-1033.

Fujita, Y. N., T. Ueno, M. Itohara, S. Yamashita, T. (2014). "Netrin-G1 Regulates Microglial Accumulation along Axons and Supports the Survival of Layer V Neurons in the Postnatal Mouse Brain." Cell Reports **31**(4).

Haynes, S. H., G. Yang, G. Kurpius, D. Dailey, ME. Gan, W. Julius, D. (2006). "The P2Y12 receptor regulates microglial activation by extracellular nucleotides." Nature Neuroscience **9**(12): 1512-1519.

Hickman, S. A., EK. El Khoury, J. (2008). "Microglial dysfunction and defective β-amyloid clearance pathways in aging Alzheimer's disease mice." J. Neurosci **28**: 8354-8360.

Hong, S. S., B. (2016). "Microglia: Phagocytosing to Clear, Sculpt, and Eliminate." Developmental Cell **38**(2): 126-128.

Johnson, E. C., EK. Dammer, EB. Duong, DM. Gerasimov, ES. Liu, Y. Liu, J. Betarbet, R. Ping, L. Yin, L. Serrano, GE. Beach, TG. Peng, J. De Jager, PL. Haroutunian, V. Zhang, B. Gaiteri, C. Bennett, DA. Gearing, M. Wingo, TS. Wingo, AP. Lah, JJ. Levey, AI. Seyfried, NT. (2022). "Large-scale deep multi-layer analysis of Alzheimer's disease brain reveals strong proteomic disease-related changes not observed at the RNA level." Nature Neuroscience **25**: 213-225

Kenkhuis, B. S., A. Kleindouwel, LRT. van Room-Mom, WMC. Hollt, T. van der Weerd, L. (2022). "Co-expression patterns of microglia markers Iba1, TMEM119 and P2RY12 in Alzheimer's disease." Neurobiol Dis **167**.

Keren-Shaul, H. S., A. Weiner, A. Matcovirch-Natan, O. Dvir-Szternfeld, R. Ulland, TK. David, E. Baruch, K. Lara-Astaiso, D. Toth, B. Itzkovitz, S. Colonna, M. Schwartz, M. Amit, I. (2017). "A Unique Microglia Type Associated with Restricting Development of Alzheimer's Disease." Cell **169**: 1276-1290.

Koss, K. C., MA. Tsui, C. Todd, KG. (2019). "In Vitro Priming and Hyper-Activation of Brain Microglia: an Assessment of Phenotypes." Mol Neurobiol **56**(9): 6409-6425.

Krasemann, S. M., C. Cialic, R. Baufeld, C. Calcagno, N. El Fatimy, R. Beckers, L. O'Loughlin, E. Xu, Y. Fanek, Z. Greco, DJ. Smith, ST. Tweet, G. Humulock, Z. Zrzavy, T. Conde-Sanroman, P. Gacias, M. Weng, Z. Chen, H. Tjon, E. Mazaheri, F. Hartmann, K. Madi, A. Ulrich, JD. Glatzel, M. Worthmann, A. Heeren, J. Budnik, B. Lemere, C. Ikezu, T. Heppner, FL. Litvak, V. Holtzmann, DM. Lassmann, H. Weiner, HL. Ochando, J. Haass, C. Butovsky, O. (2017). "The TREM2-APOE Pathway Drives the Transcriptional Phenotype of Dysfunctional Microglia in Neurodegenerative Diseases." Immunity **47**(3): 566-581.

Lauro, C. L., C. (2020). "Metabollic Reprogramming of Microglia in the Regulation of the Innate Inflammatory Response." Front Immunol **11**(493).

Li, Q. B., BA. (2018). "Microglia and macrophages in brain homeostasis and disease." Nature Reviews Immunology **18**: 225-242.

Lloyd, A. D., CL. Holloway, RK. Labrak, Y. Ireland, G. Carradori, D. Dillenburg, A. Borger, E. Soong, D. Richardson, JC. Kuhlmann, T. Williams, A. Pollard, JW. des Rieux, A. Priller, J. Miron, VE. (2019). "Central nervous system regeneration is driven by microglia necroptosis and repopulation." Nature Neuroscience **22**: 1046-1052.

Maedera, S. M., T. Ishiguro, H. Ito, T. Soga, T. Kusuhara, H. (2018). "GLUT6 is a lysosomal transporter that is regulated by inflammatory stimuli and modulates glycolysis in macrophages." FEBS Letters **593**(2): 195-208.

Mancuso, R. V. D. D., J. Fattorelli, N. Wolfs, L. Balusu, S. Burton, O. Liston, A. Sierksma, A. Fourne, Y. Poovathingalm S. Arranz-Mendiguren, A. Sala Frigerio, C. Claes, C. Serneels, L. Theys, T. Perry, VH. Verfaillie, C. Fiers, M. De Strooper, B. (2019). "Stem-cell-derived human microglia transplanted in mouse brain to study human disease." Nature Neuroscience **22**: 2111-2116.

Masuda, T. S., R. Staszewski, O. Bottcher, C. Amann, L. Sagar. Scheiwe, C. Nessler, S. Kunz, P. Van Loo, G. Coenen, VA. Reinacher, PC. Michel, A. Sure, U. Gold, R. Grun, D. Priller, J. Stadelmann, C. Prinz, M. (2019). "Spatial and temporal heterogeneity of mouse and human microglia at single-cell resolution." Nature **566**: 388-392.

McQuade, A. C., M. Tu, CH. Hasselmann, J. Davtyan, H. Blurton-Jones, M. (2018). "Development and validation of a simplified method to generate human microglia from pluripotent stem cells." Molecular Neurodegeneration **13**(67).

Minarrieta, L. V., LN. Sparwasser, T. Berod, L. (2021). "Dendritic cell metabolism: moving beyond in vitro-culture-generated paradigms." Current Opinion in Biotechnology **68**: 202-212.

Miron, V. B., A. Zhao, J. Yuen, TJ. Ruckh, JM. Shadrach, JL. van Wijngaarden, P. Wagers, AJ. Williams, A. Franklin, RJM. Ffrench-Constant, C. (2013). "M2 microglia and macrophages drive oligodendrocyte differentiation during CNS remyelination." Nature Neuroscience **16**: 1211-1218.

Monsorno, K. B., A. Paolicelli, RC. (2022). "Microglial metabolic flexibility: emerging roles for lactate." Trends in Endocrinology and Metabolism **33**(3): 186-195.

Olah, M. P., E. Villani, A. Xu, J. White, CC. Ryan KJ. Piehowski, P. Kapasi, A. Nejad, P. Cimpean, M. Connor, S. Yung, CJ. Frangeih, M. McHenry, A. Elyaman, W. Petyuk, V. Schneider, JA. Bennett, DA. De Jager, PL. Bradshaw, EM. (2018). "A transcriptomic atlas of aged human microglia." Nature Communications **9**.

Pollock, T. C., GN. Isho, NF. Day, RJ. Suresh, T. Stewart, ES. McCarthy, MM. Rohn, TT. (2020). "Transcriptome Analyses in BV2 Microglial Cells Following Treatment With Amino-Terminal Fragments of Apolipoprotein E." Front. Aging Neurosci **13**.

Pont-Lezica, L. B., W. Colasse, S. Drexhage, H. Versnel, M. Bessis, A. (2014). "Microglia shape corpus callosum axon tract fasciculation: functional impact of prenatal inflammation." Eur J Neurosci **39**(10): 1551-1557.

Rossi, F. C., AM. Henke, K. Richter, K. Peri, F. (2015). "The SLC7A7 Transporter Identifies Microglial Precursors prior to Entry into the Brain." Cell Reports **19**(7): 1008-1017.

Serneels, L. T. S., D. Perez-Benito, L. Theys, T. Holt, MG. De Strooper, B. (2020). "Modeling the β-secretase cleavage site and humanizing amyloid-beta precursor protein in rat and mouse to study Alzheimer's disease." Molecular Neurodegeneration **60**: 1-11.

Serrano-Pozo, A. G.-I., T. Growdon, JH. Frosch, MP. Hyman, BT. (2013). "A phenotypic change but not proliferation underlies glial responses in Alzheimer disease." Am. J. Pathol **182**: 2332-2344.

Shafer, D. L., EK. Kautzman, AG. Koyama, R. Mardinly, AR. Yamasaki, R. Ransohoff, RM. Greenberg, ME. Barres, BA. Stevens, B. (2012). "Microglia Sculpt Postnatal Neural Circuits in an Activity and Complement-Dependent Manner." Neuron **74**(4): 691-705.

Squarzoni, P. O., G. Hoeffel, G. Pont-Lezica, L. Rostaing, P. Low, D. Bessis, A. Ginhoux, F. Garel, S. (2014). "Microglia modulate wiring of the embryonic forebrain." Cell Reports **11**(5): 1271-1279.

Steenbergen, R. O., M. ter Host, R. Tat, W. Neufeldt, C. Belovodskiy, A. Chua, TT. Cho, WJ. Joyce, M. Dutilh, BE. Tyrrell, DL. (2018). "Establishing normal metabolism and differentiation in hepatocellular carcinoma cells by culturing in adult human serum." Scientific Reports **8**.

Stevens, B. A., NJ. Vazquez, LE. Howell, GR. Christopherson, KS. Nouri, N. Micheva, KD. Mehalow, AK. Huberman, AD. Stafford, B. Sher, A. Litke, AM. Lambris, JD. Smith, SJ. John, SWM. Barres, BA. (2007). "The Classical Complement Cascade Mediates CNS Synapse Elimination." Cell **131**(6): 1164-1178.

Suzuki, C. G., RG. Edmonds, KA. Hiller, S. Hyberts, SG. Marintchev, A. Wagner, G. (2008). "PDCD4 inhibits translation initiation by binding to eIF4A using both its MA3 domains." Proc Natl Acad Sci U S A **105**(9): 3274-3279.

Suzumura, A. S., M. Yamamoto, H. Marunouchi, T. (1993). "Transforming growth factor-beta suppresses activation and proliferation of microglia in vitro." J Immunol **151**(4): 2150-2158.

Ueno, M. F., Y. Tanaka, T. Nakamura, Y. Kikuta, J. Ishii, M. Yamashita, T. (2013). "Layer V cortical neurons require microglial support for survival during postnatal development." Nature Neuroscience **16**: 543-551.

Wisniewski, J. H., MY. Cox, J. Mann, M. (2014). "A "proteomic ruler" for protein copy number and concentration estimation without spike-in standards." Mol Cell Proteomics **13**(12): 3497-3506.

Wlodarczyk, A. H., IR. Krueger, M. Yogev, N. Bruttger, J. Khorooshi, R. Benmamar-Badel, A. de Boer-Bergsma, JJ. Martin, NA. Karram, K. Kramer, I. Boddeke, EWGM. Waisman, S. Eggen, BJL. Owens, T. (2017). "A novel microglial subset plays a key role in myelinogenesis in developing brain." The Embo Journal **36**: 3292-3308.

Xing, H. H., H. Gelpi, E. Kubota, R. Budka, H. Izumo, S. (2009). "Reduced expression of excitatory amino acid transporter 2 and diffuse microglial activation in the cerebral cortex in AIDS cases with or without HIV encephalitis." J Neuropathol Exp Neurol **68**(2): 199-209.

Yoon, B. O., Y. Kang, SW. Lee, EB. Lee, W. (2018). "Role of SLC7A5 in Metabolic Reprogramming of Human Monocyte/Macrophage Immune Responses." Front Immunol **9**.

Zhang, Y. C., K. Sloan, SA. Bennett, ML. Scholze, AR. O'Keeffe, S. Phatnani, HP. Guarnieri, P. Caneda, C. Ruderisch, N. Deng, S. Liddelow, SA. Zhang, C. Daneman, R. Maniatis, T. Barres, BA. Qian Wu, J. (2014). "An RNA-Sequencing Transcriptome and Splicing Database of Glia, Neurons, and Vascular Cells of the Cerebral Cortex." Journal of Neuroscience **34**: 11929-11947.

Zoller, T. S., A. Kleimeyer, C. Masuda, T. Sankar Potru, P. Pfeifer, D. Blank, T. Prinz. M. Spittau, B. (2018). "Silencing of TGFβ signalling in microglia results in impaired homeostasis." Nature Communications **9**(1).

Zrzavy, T. H., S. Wimmer, I. Butovsky, O. Weiner, HL. Lassmann, H. (2017). "Loss of 'homeostatic' microglia and patterns of their activation in active multiple sclerosis." Brain **140**(7): 1900-1913.

## Figure Legends

**Figure 1. a)** Schematic of the microglia subsets and processing methods for proteomics. Biological replicates for *ex vivo* primary human microglia (n=5), *in vitro* hESC-microglia (n=3), *ex vivo* primary mouse microglia (n=4) and *in vitro* BV2 microglia (n=3) were used throughout all analyses. **b)** Total number of proteins detected in each microglia subset ±SEM. **c)** Protein mass of each microglia subset, measured in picograms (pg) per cell ±SEM. **d)** Principle component analysis of each replicate in each microglia subset. Green dots = BV2 microglia (BV2_1-3), purple dots = hESC-derived microglia (hESC_1-3), blue dots = *ex vivo* primary human microglia (hMG_1-5), yellow dots = *ex vivo* primary mouse microglia (mMG_1-4). **e)** Total protein content of proteins associated with glycolysis, mitochondria, ribosomes and nuclear envelope, measured in micrograms (µg) per million cells. **f)** Pie charts showing the proportions of the proteome dedicated to glycolysis, ribosomes, mitochondria, nuclear envelope and histone proteins for each microglia subset. Proportions were calculated by determining the percentage of protein content of each of these groups as a proportion of the total protein mass of all proteins in each microglia subset.

**Figure 2. a)** Bubble plot displaying the top 100 most abundant proteins in the *ex vivo* human microglia proteome in order of abundance. The size of the circles represent the abundance of the proteins with the most abundant proteins having the largest sized circles. **b)** Gene ontology (GO) terms for the proteins identified in *ex vivo* human microglia found in at least 3 out of 5 biological replicates. GO terms are divided into those associated with molecular function (green), cellular component (blue) and biological process (orange). **c)** Volcano plot comparing the differentially expressed proteins of *ex vivo* mouse and human samples. Red circles represent those that are significantly enriched ($Log_2FC$ >1, $-Log_{10}(P)$ >1.3). **d)** Venn diagram of the shared and differentially identified proteins (found in at least 3 biological replicates) in *ex vivo* mouse and human microglia, with examples of uniquely identified proteins in mouse (green square) and human (blue square). **e)** Concentration of APOE, CLU and SORL1 proteins in *ex vivo* mouse and human microglia ±SEM. **P<0.01, ****P<0.0001 (Two-tailed T-test). **f)** *Concentration* of IL-18 and PTPRC (CD45) proteins in *ex vivo* mouse and human microglia ±SEM. *P<0.05, ****P<0.0001 (Two-tailed T-test).

**Figure 3. a)** Homeostatic vs activated microglia and examples of their defining characteristics. **b)** Heatmap of homeostatic microglia proteins. Relative protein abundance is graded from low (blue) to high (yellow). **c-e)** Concentration of CD68, SLC2A5 and SLC2A6 in each microglia subset in nanomolars (nM) ±SEM. **f)** Schematic of the TGF-β pathway involving SMAD activation. **g-k)** Concentration (nM) of TGFBR1, TGFBR2, SMAD2, SMAD3 and SMAD4 in each microglia subset ±SEM.

**Figure 4. a)** Homeostatic, stage 1 DAM and stage 2 DAM microglia. **b)** Concentration (nM) of homeostatic microglia proteins P2RY12, TMEM119 and CX3CR1 in each microglia subset ±SEM. **c)** Concentration (nM) of stage 1 DAM signature proteins APOE, B2M, CTSB, CTSD, FTH1, TYROBP in each microglia subset ±SEM. **d)** Concentration (nM) of stage 2 DAM signature proteins CD9, CLEC7A, CSF1, ITGAX, LIPA, LILRB4, LPL, TIMP2, TREM2 in each microglia subset ±SEM.

**Figure 5. a)** The different facets of the microglia sensome. **b-e)** Concentration (nM) of SLC1A2, SLC1A3, C3 and C3CR1 in each microglia subset. **f)** Protein copy numbers of TLR3 and TLR4 in each microglia subset. **g)** Protein copy numbers of lactate transporter SLC16A1, glucose transporters SLC2A5 and SLC2A6, amino acid transporters SLC7A5 and SLC7A7 and mitochondrial solute transporters SLC25A3 and SLC25A5 for each microglia subset ±SEM.

**Figure 6. a)** Schematic of the *in vitro* and xenografted hESC-microglia and *ex vivo* human microglia samples analysed by mass spectrometry. **b)** PCA plot of each replicate including the new xenografted

microglia (labelled Xplant_1-3) biological replicates (n=3). **c)** Total protein content of samples measured as picograms per cell for *in vitro* and xenografted hESCs and *ex vivo* human microglia ±SEM. **d-f)** Proportion of total protein mass of glycolysis, mitochondria, and ribosome proteins for *in vitro* and xenografted hESCs and *ex vivo* human microglia ±SEM. **g)** Volcano plots comparing the differentially expressed proteins in *in vitro* hESCs, xenografted hESCs and *ex vivo* human microglia. Proteins highlighted in green are those associated with DAM signature in microglia (DAM). Proteins highlighted in red are those associated with microglia homeostasis (HM). **h-j)** Concentration (nM) of TMEM119, P2RY12 and CX3CR1 in *in vitro* and xenografted hESCs and *ex vivo* human microglia ±SEM.

**Supplemental Figure 1. a)** Venn diagram of the shared and uniquely identified proteins in BV2, *in vitro* hESC-microglia, *ex vivo* mouse and *ex vivo* human microglia. hESC = hESC derived microglia, hMG = *ex vivo* primary human microglia, BV2 = BV2 microglia, mMG = *ex vivo* primary mouse microglia. **b)** Protein content of histones in each microglia subset ±SEM. **c)** Gene ontology (GO) terms of proteins conserved across all microglia subtypes. **d)** Schematic of the eukaryotic initiation factor (eIF) complex. **e)** Concentration (nM) of eIF proteins eIF4G1, eIF4E, eIF4A1 and inhibitor PDCD4 in each microglia subset ±SEM. **f)** Average copy numbers of PDCD4 and eIF4A1, the average ratio and adjusted ratio (1 PDCD4 molecule to 2 eIF4A1 molecules) of these proteins.

**Supplemental Figure 2. a)** Number of proteins detected in each biological replicate of *ex vivo* human microglia. **b)** Protein mass (picograms per cell) for each biological replicate of *ex vivo* human microglia. **c)** Venn diagram of shared and unique proteins in each biological replicate of *ex vivo* human microglia. **d)** Table of the top 20 most abundant proteins in *ex vivo* microglia with the average copy number across all 5 biological replicates. **e)** Table of significantly enriched GO terms in *ex vivo* human microglia compared to *ex vivo* mouse microglia.

**Supplemental Figure 3. a)** Volcano plot of the differentially expressed proteins in *ex vivo* mouse and BV2 microglia displayed as protein copy numbers. Vertical lines show mean fold change (grey) and ±2x standard deviation of the mean fold change (red). **b)** Volcano plot of the differentially expressed proteins in *ex vivo* mouse and BV2 microglia displayed as protein concentration. **c)** Total protein content per cell (pg) of BV2 cells that underwent direct lysis on plate (lysis) compared to FACS sorted BV2s that were either stained to unstained. **d)** Number of proteins detected in BV2 cells directly lysed, FACS sorted and stained or unstained. **e)** Venn diagram displaying the similarities in proteins detected across sorted and unsorted BV2 cells.

**Supplemental Figure 4. a)** Volcano plots comparing the differentially expressed proteins in *in vitro* hESCs, xenografted hESCs and *ex vivo* human microglia. All highlighted proteins are significantly enriched ($Log_2FC > 1$, $-Log_{10}(P) > 1.3$).

# Figure 1

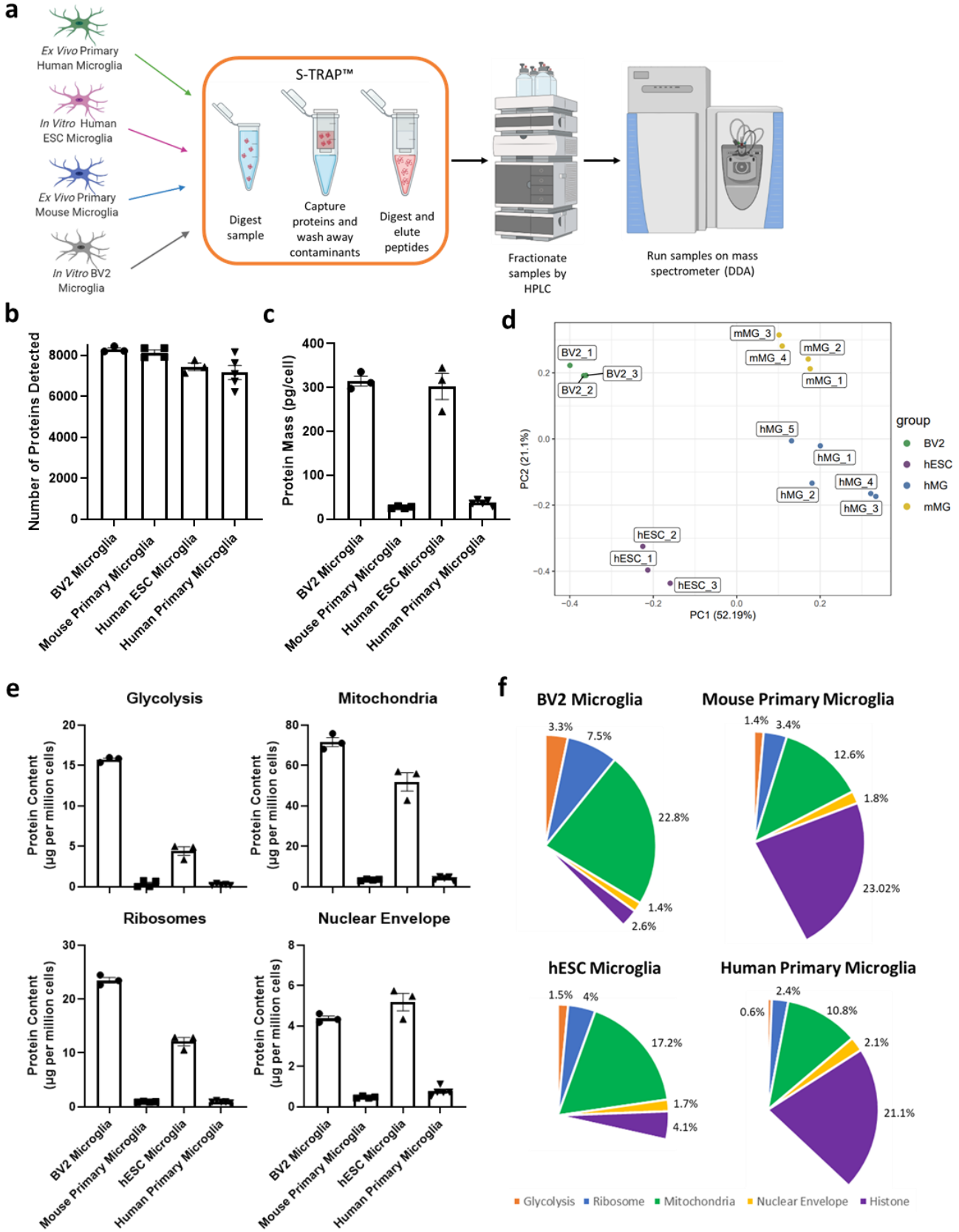

# Figure 2

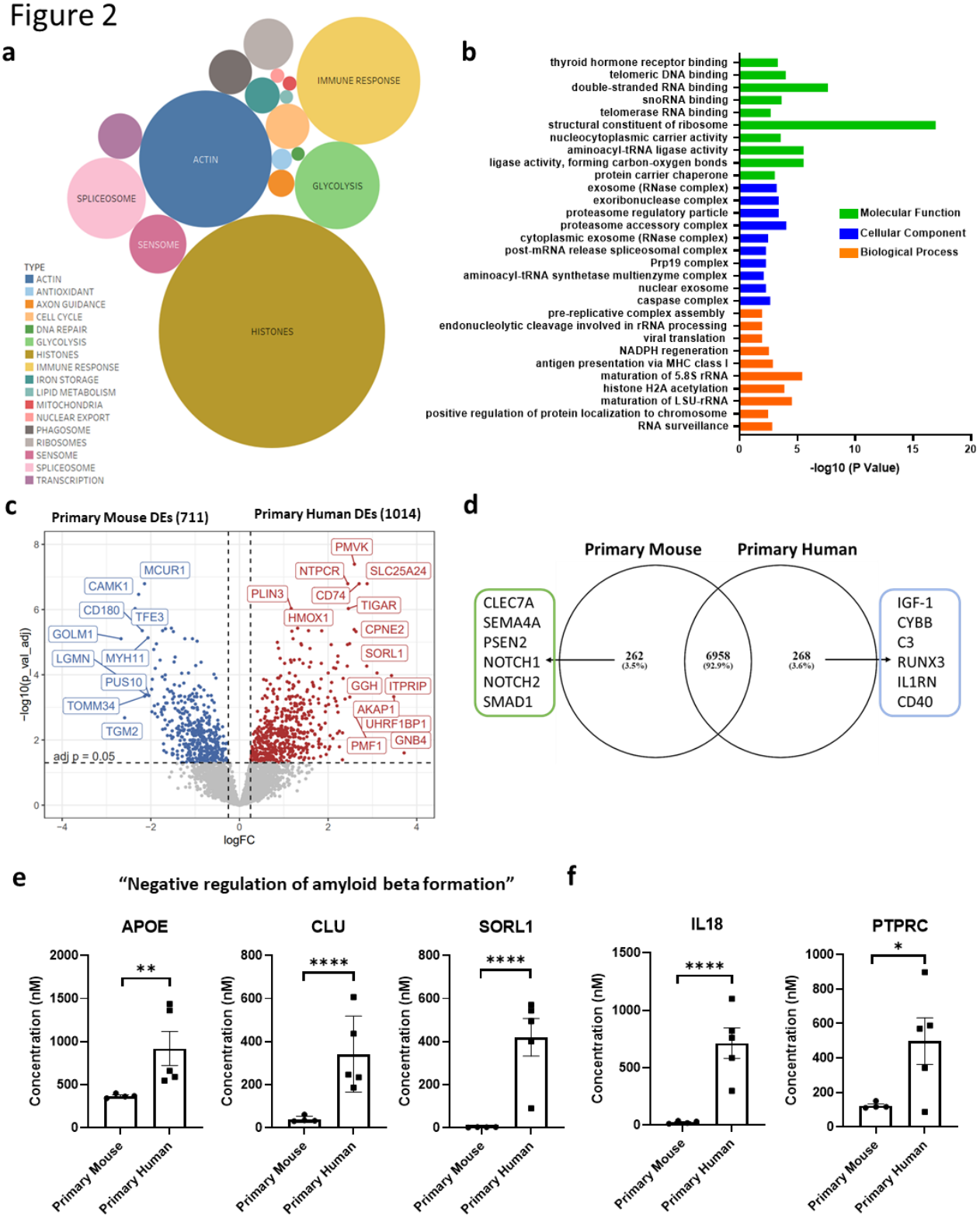

# Figure 3

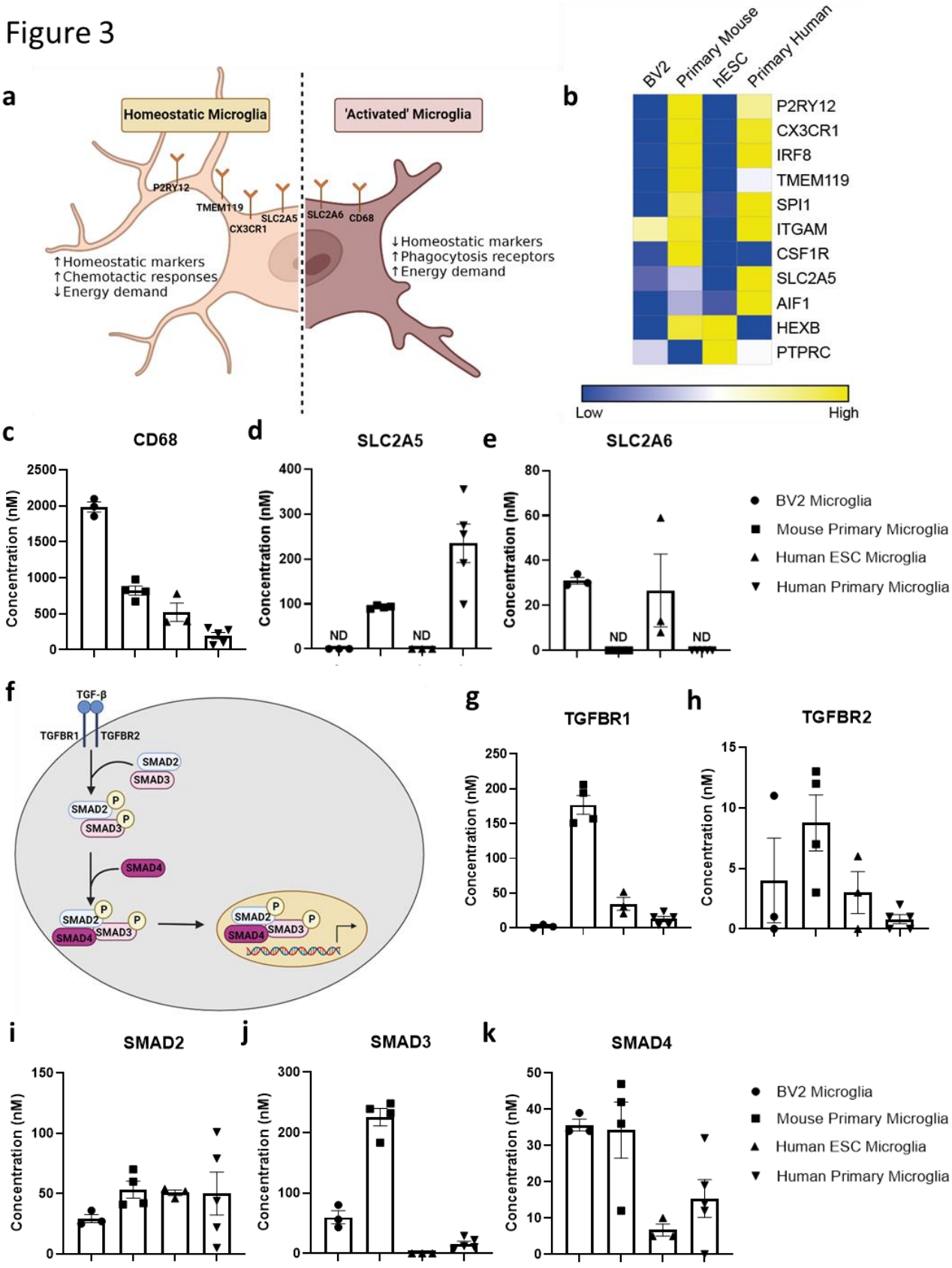

Figure 4

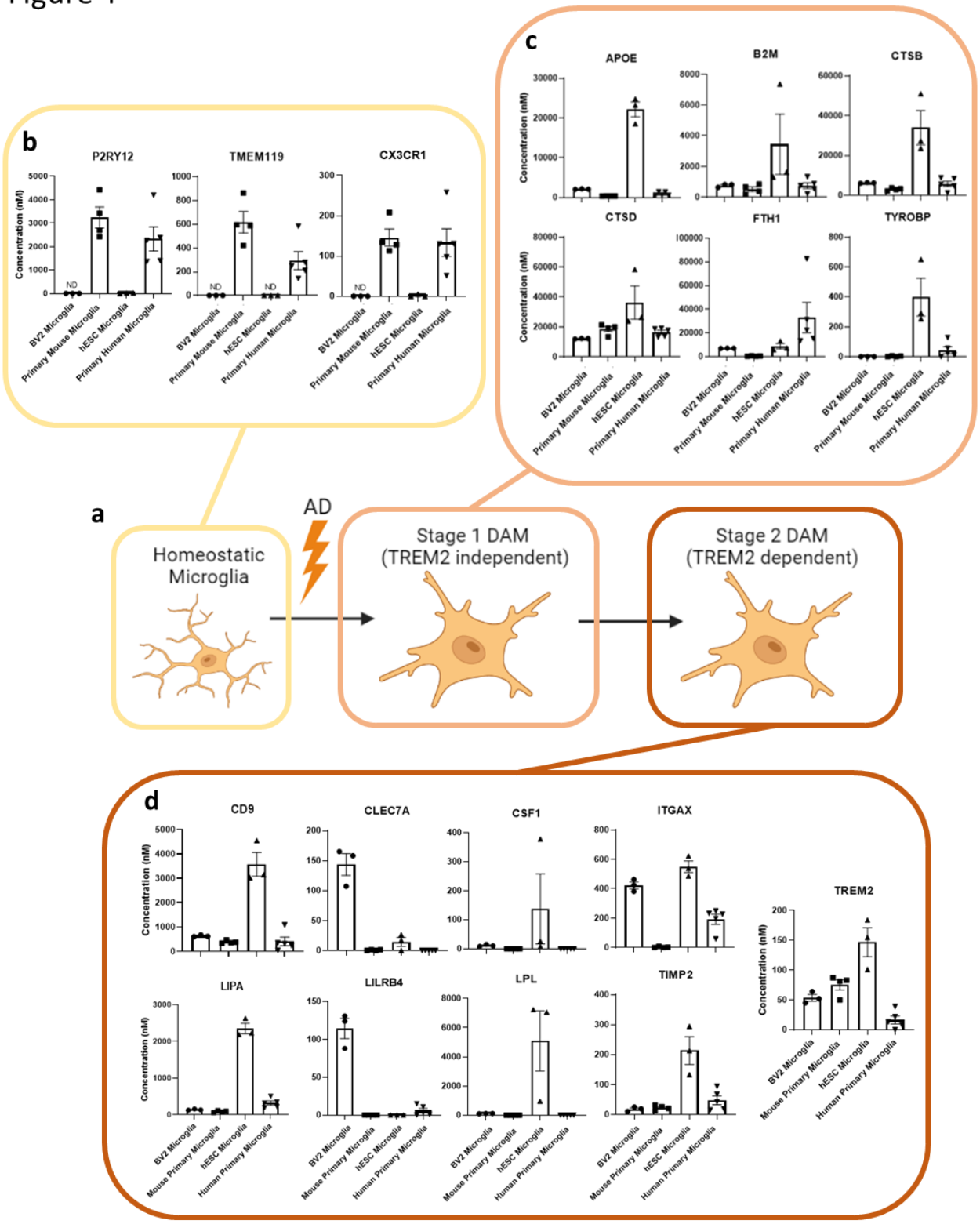

# Figure 5

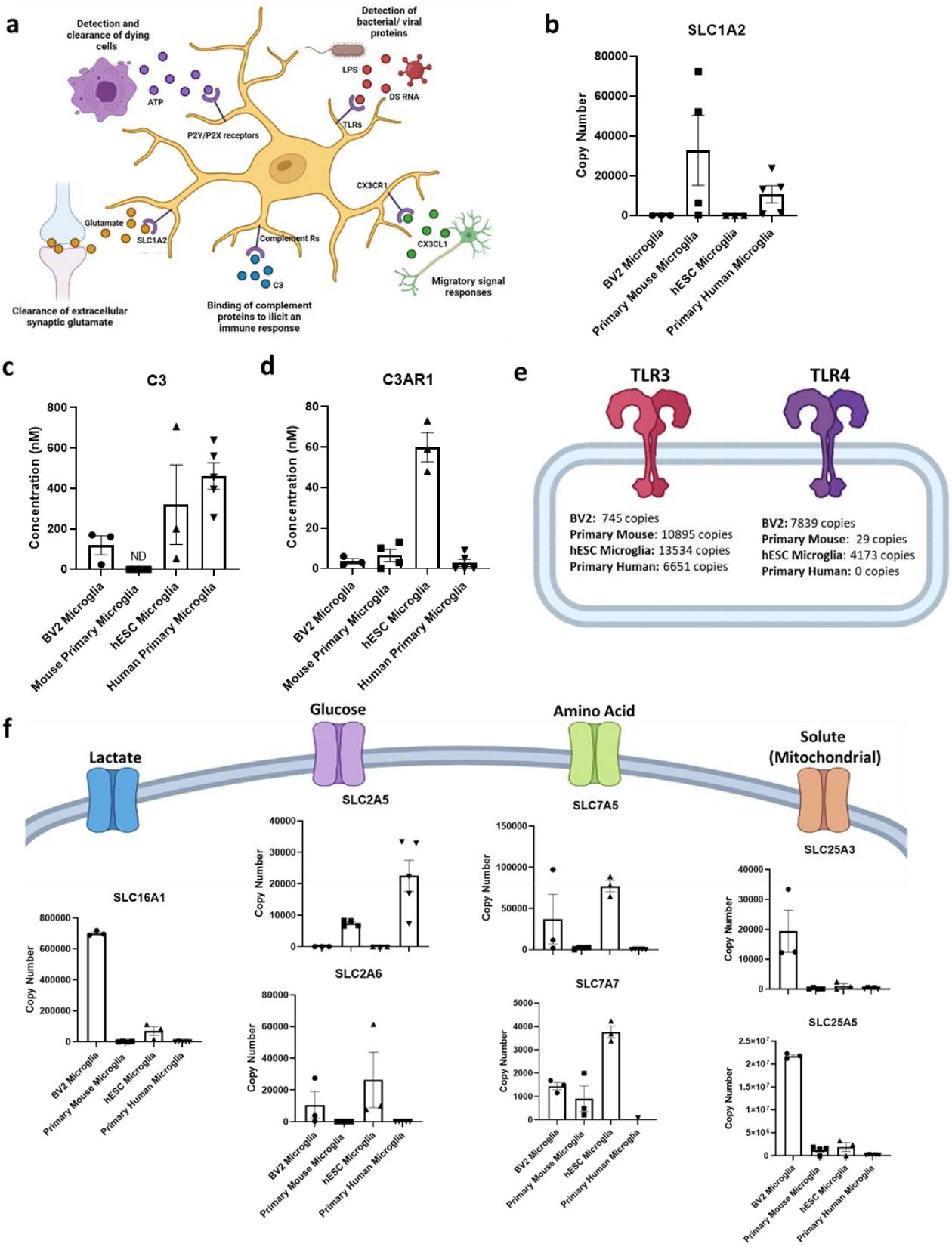

# Figure 6

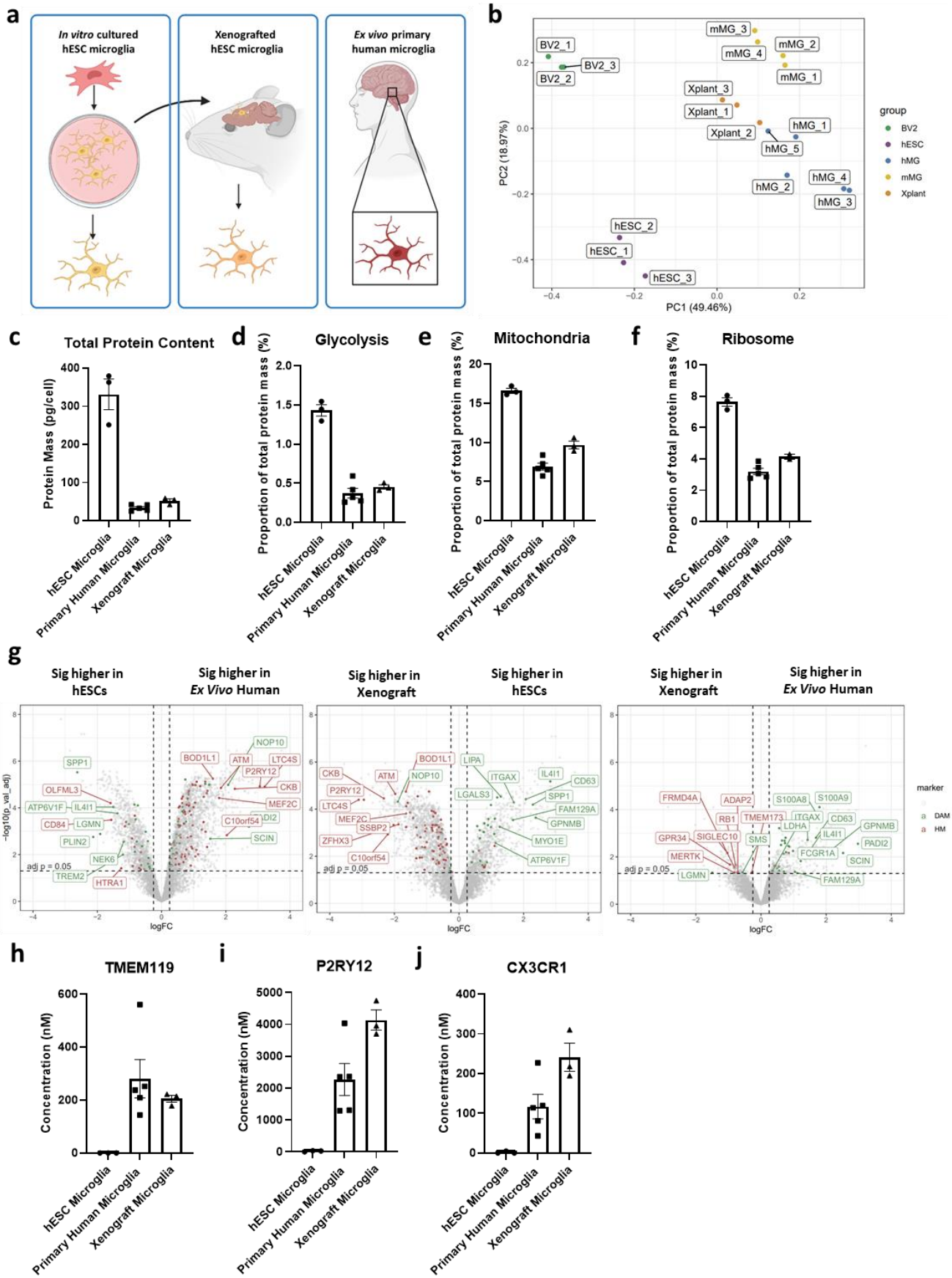

# Supplemental Fig 1

**a**

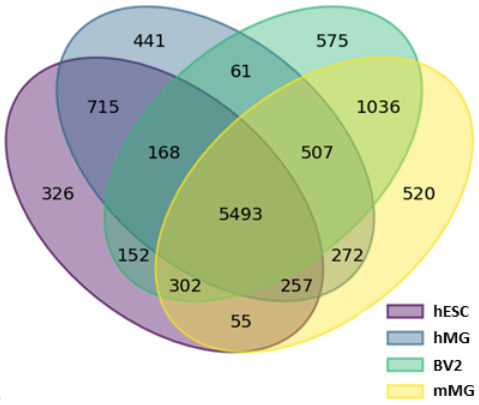


**b**

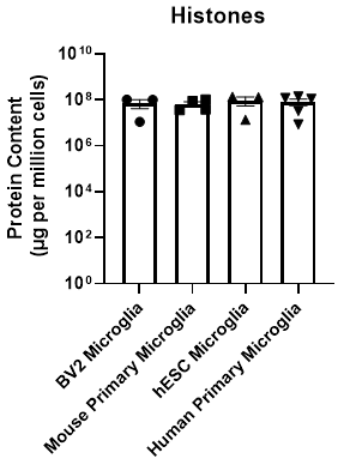


**c**

| GO biological process complete | Fold Enrichment | raw P-value | FDR |
|---|---|---|---|
| protein deneddylation (GO:0000338) | 4.35 | 1.51E-03 | 2.41E-02 |
| retrograde transport, vesicle recycling within Golgi (GO:0000301) | 4.35 | 2.60E-03 | 3.78E-02 |
| ncRNA export from nucleus (GO:0097064) | 4.35 | 2.60E-03 | 3.77E-02 |
| antigen processing and presentation of exogenous peptide antigen via MHC class I, TAP-dependent | 4.1 | 9.72E-05 | 2.37E-03 |
| RNA surveillance (GO:0071025) | 4.06 | 2.81E-04 | 5.97E-03 |
| ribosome localization (GO:0033750) | 4.02 | 8.16E-04 | 1.47E-02 |
| glycolytic process through glucose-6-phosphate (GO:0061620) | 4.02 | 8.16E-04 | 1.46E-02 |
| NADH regeneration (GO:0006735) | 3.96 | 2.40E-03 | 3.54E-02 |
| phosphorylation of RNA polymerase II C-terminal domain (GO:0070816) | 3.96 | 2.40E-03 | 3.54E-02 |
| glucose catabolic process to pyruvate (GO:0061718) | 3.96 | 2.40E-03 | 3.54E-02 |

**d**

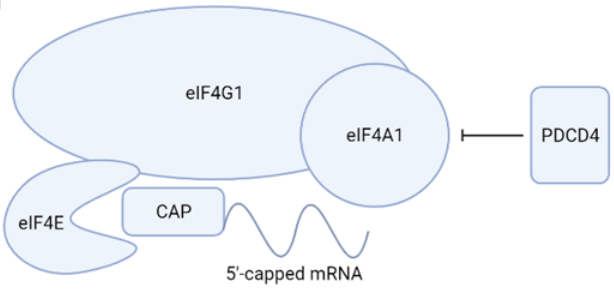


**e**

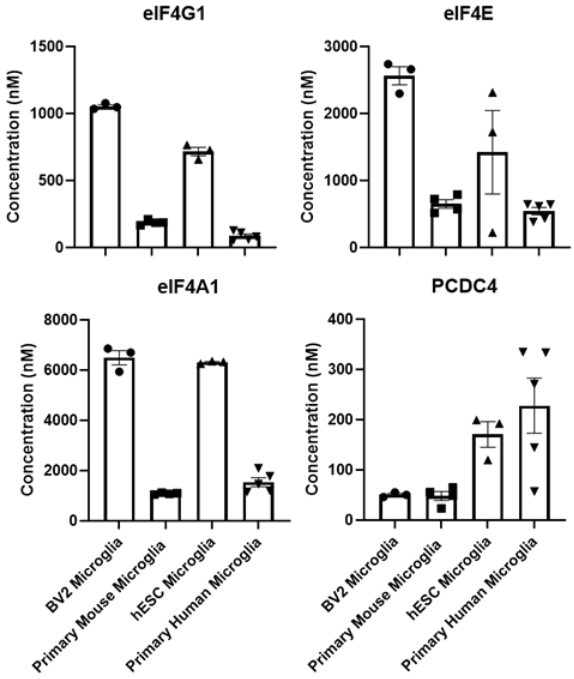


**f**

| | Average PDCD4 Copy Number | Average eIF4A1 Copy Number | Average Ratio | Adjusted Ratio |
|---|---|---|---|---|
| **BV2 Microglia** | 47,669 | 6,140,936 | 1:128 | 1:64 |
| **Mouse Primary Microglia** | 3,879 | 86856 | 1:22 | 1:11 |
| **hESC Microglia** | 151,669 | 5,730,136 | 1:37 | 1:19 |
| **Human Primary Microglia** | 23,043 | 149,691 | 1:6 | 1:3 |

# Supplemental Fig 2

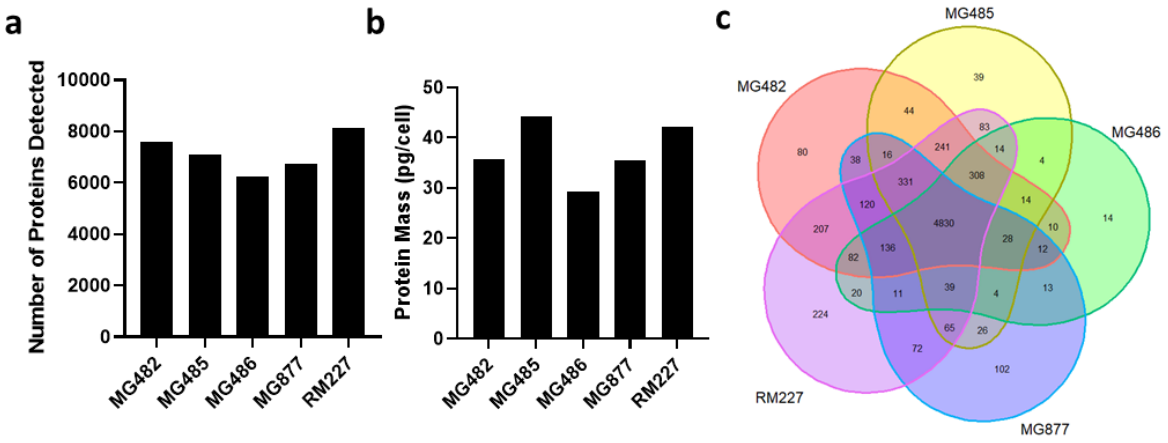


**d**

| TOP 20 Most Abundant Primary Human Microglia Proteins | | |
|---|---|---|
| **Gene names** | **Protein names** | **Average Copy Number** |
| HIST1H4A | Histone H4 | 70649403.8 |
| ACTB | Actin | 18587115.8 |
| H3F3A | Histone H3.3 | 17090863 |
| S1A9 | Protein S1-A9 | 14953368.4 |
| H1F | Histone H1 | 9489718.4 |
| HIST1H1E | Histone H1.4 | 8389364.6 |
| TMSB4X | Thymosin beta-4 | 6996802.2 |
| RPS27A | Ubiquitin-4S ribosomal protein S27a | 4942567.8 |
| PFN1 | Profilin-1 | 4621031.6 |
| S1A8 | Protein S1-A8 | 4179937 |
| GAPDH | Glyceraldehyde-3-phosphate dehydrogenase | 3789068.2 |
| FTH1 | Ferritin heavy chain | 2677053.6 |
| HNRNPC | Heterogeneous nuclear ribonucleoproteins C1/C2 | 2673634 |
| TUBA1B | Tubulin alpha-1B chain | 2498320.4 |
| PRDX1 | Peroxiredoxin-1 | 2326158.6 |
| CFL1 | Cofilin-1 | 2176894 |
| H2AFY | Core histone macro-H2A.1 | 2152696 |
| TPM3 | Tropomyosin alpha-3 chain | 2104441 |
| TKT | Transketolase | 2066265 |
| HP1BP3 | Heterochromatin protein 1-binding protein 3 | 2060466.4 |

**e**

| Significantly enriched Primary Human Microglia GO TERMS | Fold Enrichment | Raw P-value | FDR |
|---|---|---|---|
| Regulation of fc-gamma receptor signalling pathway involved in phagocytosis | 28.56 | 7.14E-04 | 3.62E-02 |
| Regulation of neurofibrillary tangle assembly | 28.56 | 7.14E-04 | 3.61E-02 |
| Positive regulation of fc receptor mediated stimulatory signalling pathway | 22.85 | 1.43E-04 | 1.06E-02 |
| Negative regulation of amyloid-beta formation | 7.93 | 8.85E-04 | 4.33E-02 |
| Regulation of neuroinflammatory response | 4.5 | 9.35E-04 | 4.24E-02 |
| Regulation of macrophage activation | 3.73 | 4.47E-04 | 2.33E-02 |

# Supplemental Fig 3

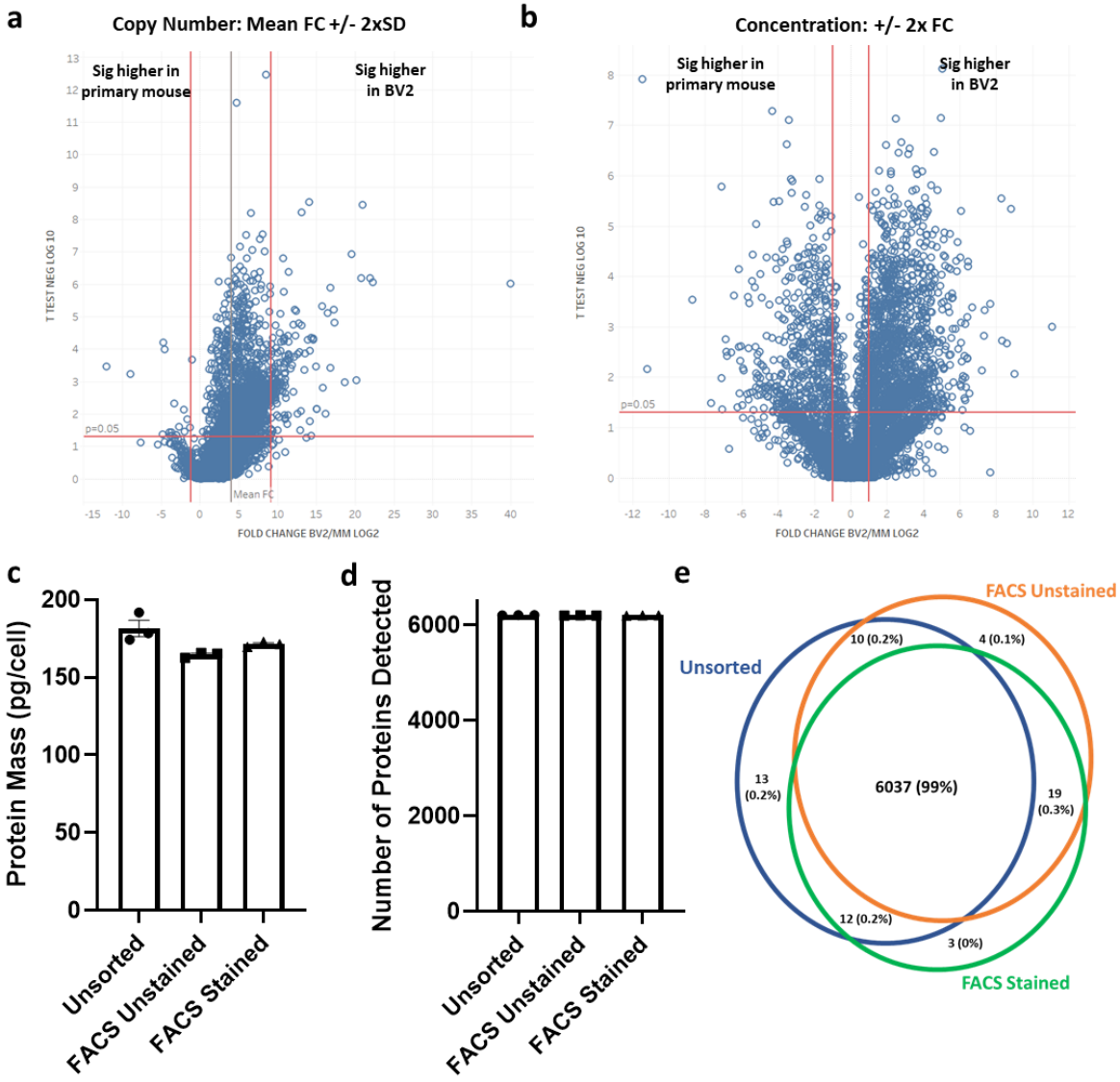

# Supplemental Fig 4